AGU100 ADVANCING EARTH AND SPACE SCIENCE

JGR

Journal of Geophysical Research: Atmospheres

RESEARCH ARTICLE

10.1029/2017JD028082

Special Section:
Winter INvestigation of Transport, Emissions and Reactivity (WINTER)

Ben H. Lee and Felipe D. Lopez-Hilfiker contributed equally to this work.

Key Points:
- Series of upgrades implemented on the University of Washington aircraft-based HRToF-CIMS improves accuracy and robustness of measurements
- We report on the detection of HCl, SO_2, $ClNO_2$, and a suite of reactive halogen and nitrogen oxide species utilizing iodide adduct ionization
- Observations from WINTER (Cl,Br species in coal-fired power plant exhaust and full speciation of NO_z species) are presented as examples

Supporting Information:
- Supporting Information S1

Correspondence to:
J. A. Thornton,
thornton@atmos.washington.edu

Citation:
Lee, B. H., Lopez-Hilfiker, F. D., Veres, P. R., McDuffie, E. E., Fibiger, D. L., Sparks, T. L., et al. (2018). Flight deployment of a high-resolution time-of-flight chemical ionization mass spectrometer: Observations of reactive halogen and nitrogen oxide species. *Journal of Geophysical Research: Atmospheres*, *123*, 7670–7686. https://doi.org/10.1029/2017JD028082

Received 20 NOV 2017
Accepted 24 JUN 2018
Accepted article online 2 JUL 2018
Published online 21 JUL 2018

©2018. American Geophysical Union. All Rights Reserved.

Flight Deployment of a High-Resolution Time-of-Flight Chemical Ionization Mass Spectrometer: Observations of Reactive Halogen and Nitrogen Oxide Species

Ben H. Lee[1], Felipe D. Lopez-Hilfiker[1], Patrick R. Veres[2], Erin E. McDuffie[2,3,4], Dorothy L. Fibiger[2], Tamara L. Sparks[5], Carlena J. Ebben[5], Jaime R. Green[6,7], Jason C. Schroder[3,4], Pedro Campuzano-Jost[3,4], Siddharth Iyer[8], Emma L. D'Ambro[1,9], Siegfried Schobesberger[1,10], Steven S. Brown[2,4], Paul J. Wooldridge[5], Ronald C. Cohen[5], Marc N. Fiddler[7], Solomon Bililign[6,7], Jose L. Jimenez[3,4], Theo Kurtén[8], Andrew J. Weinheimer[11], Lyatt Jaegle[1], and Joel A. Thornton[1]

[1]Department of Atmospheric Sciences, University of Washington, Seattle, WA, USA, [2]Chemical Sciences Division, Earth System Research Laboratory, National Oceanic and Atmospheric Administration, Boulder, CO, USA, [3]Cooperative Institute for Research in Environmental Sciences, University of Colorado Boulder, Boulder, CO, USA, [4]Department of Chemistry and Biochemistry, University of Colorado Boulder, Boulder, CO, USA, [5]Department of Chemistry, University of California, Berkeley, CA, USA, [6]Department of Physics, North Carolina A and T State University, Greensboro, NC, USA, [7]NOAA-ISET Center, North Carolina A and T State University, Greensboro, NC, USA, [8]Department of Chemistry, University of Helsinki, Helsinki, Finland, [9]Department of Chemistry, University of Washington, Seattle, WA, USA, [10]Now at Department of Applied Physics, University of Eastern Finland, Kuopio, Finland, [11]National Center for Atmospheric Research, Boulder, CO, USA

Abstract We describe the University of Washington airborne high-resolution time-of-flight chemical ionization mass spectrometer (HRToF-CIMS) and evaluate its performance aboard the NCAR-NSF C-130 aircraft during the recent Wintertime INvestigation of Transport, Emissions and Reactivity (WINTER) experiment in February–March of 2015. New features include (i) a computer-controlled dynamic pinhole that maintains constant mass flow-rate into the instrument independent of altitude changes to minimize variations in instrument response times; (ii) continuous addition of low flow-rate humidified ultrahigh purity nitrogen to minimize the difference in water vapor pressure, hence instrument sensitivity, between ambient and background determinations; (iii) deployment of a calibration source continuously generating isotopically labeled dinitrogen pentoxide ($^{15}N_2O_5$) for in-flight delivery; and (iv) frequent instrument background determinations to account for memory effects resulting from the interaction between sticky compounds and instrument surface following encounters with concentrated air parcels. The resulting improvements to precision and accuracy, along with the simultaneous acquisition of these species and the full set of their isotopologues, allow for more reliable identification, source attribution, and budget accounting, for example, by speciating the individual constituents of nocturnal reactive nitrogen oxides ($NO_z = ClNO_2 + 2 \times N_2O_5 + HNO_3$ + etc.). We report on an expanded set of species quantified using iodide-adduct ionization such as sulfur dioxide (SO_2), hydrogen chloride (HCl), and other inorganic reactive halogen species including hypochlorous acid, nitryl chloride, chlorine, nitryl bromide, bromine, and bromine chloride (HOCl, $ClNO_2$, Cl_2, $BrNO_2$, Br_2, and BrCl, respectively).

1. Introduction

Advancements in instrument development to improve observational capability are essential for monitoring and understanding environmental change. Though trace gases represent a small mass fraction of the atmosphere, they are composed of thousands of unique constituents (Goldstein & Galbally, 2007; Kroll et al., 2011) that influence the climate, air quality, and human and ecosystem health. Given the uncertainty associated with their molecular identities and functional classes, an instrument with selectivity toward a greater number of compounds can provide a more complete view of their interactions, which is essential in studying atmospheric chemistry where couplings can involve many species across a range of timescales. Since various trace gas abundances can range from several parts per billion (ppb) to below parts per trillion (ppt), the ability to quantify their impact is facilitated by improvements to instrument sensitivity and detection limits under a variety of operating conditions. Characterizing atmospheric variability on relevant spatial scales often requires deployment on fast-moving airborne platforms, which, in turn, imposes further restrictions on

size, weight, and power consumption. Rapid changes in the ambient air encountered during flight also requires instrument response times faster than 1 Hz, which poses a challenge to robustly measuring species such as nitric acid (HNO_3) and dinitrogen pentoxide (N_2O_5) that physically and/or chemically interact with sampling surfaces, thereby, degrading their response times and quantification.

The University of Washington high-resolution time-of-flight chemical ionization mass spectrometer (henceforth, HRToF-CIMS) has demonstrated selectivity, sensitivity, portability, and time response capable of mixing ratio and eddy covariance flux measurements under conditions ranging from pristine to polluted atmosphere (D'Ambro et al., 2017; Lopez-Hilfiker, Mohr, et al., 2016; Mohr et al., 2017; Schobesberger et al., 2016). Here we present on the aircraft deployable version, first described in Lee et al. (2014), but which has undergone substantial upgrades. We demonstrate the instrument capability in detecting sulfur dioxide (SO_2), hydrogen chloride (HCl), and a series of inorganic reactive halogen species (RHS) including hypochlorous acid, nitryl chloride, chlorine, nitryl bromide, bromine, and bromine chloride (HOCl, $ClNO_2$, Cl_2, $BrNO_2$, Br_2, and BrCl, respectively) using iodide-adduct ionization mass spectrometry.

RHS readily photolyze to generate chlorine and bromine radicals that initiate oxidation, thereby influencing the ambient abundances of volatile organic compounds, nitrogen oxides (NO_x), ozone (O_3), and mercury (Hg) (Chang & Allen, 2006; Faxon et al., 2015; Tanaka et al., 2003). Yet the emission, secondary production, and tropospheric fate of these photolabile reservoir species have been explored in limited regions and seasons (Finlayson-Pitts, 2003, 2010; Platt & Hönninger, 2003; Rossi, 2003; Saiz-Lopez & von Glasow, 2012; Simpson et al., 2015). The activation of surface-bound chloride by N_2O_5 resulting in elevated levels of $ClNO_2$ in moderately polluted nighttime atmospheres both near and far from coastal regions (Mielke et al., 2011; Osthoff et al., 2008; Riedel et al., 2012, 2013; Thornton et al., 2010; Young et al., 2012) underscores a pathway by which RHS influence the transport and transformation of oxidants and NO_x (Riedel et al., 2014; Sarwar et al., 2014; Wang et al., 2016). The measurement of subsets of these RHS using iodide-adduct ionization (Faxon et al., 2015; Huey et al., 1995; Kercher et al., 2009; Liao et al., 2011, 2014; McNeill et al., 2006; Neuman et al., 2010; Osthoff et al., 2008; Riedel et al., 2012, 2013; Roberts et al., 2008, 2010; Thornton & Abbatt, 2005) and other ionization methods (Finley & Saltzman, 2006; Foster et al., 1999; Huey et al., 1995; Jurkat et al., 2010; Lawler et al., 2011; Marcy et al., 2005; Spicer et al., 1998) is well established. The technique described herein simultaneously measures HCl, HOCl, $ClNO_2$, Cl_2, $BrNO_2$, Br_2, and BrCl, along with their stable isotopologues that provide additional constraints to their identification. Observation of HCl, typically the most abundant of the inorganic chlorine reservoir species, is particularly advantageous as existing mass spectrometric methods have limited application in the troposphere due to interfering ionization reactions with water vapor (Arnold & Viggiano, 2001; Huey et al., 1995, 2004; Marcy et al., 2005; Slusher et al., 2004) or other chlorine containing species (Roberts et al., 2010).

A major source of RHS over inland regions is coal-fired power plants (PPs; McCulloch et al., 1999), the dominant source of atmospheric SO_2 (Bates et al., 1992; Smith et al., 2011). As such, measuring SO_2 alongside a suite of RHS provides a robust approach to characterizing coal-fired PP emissions. SO_2 is removed from the atmosphere primarily by homogeneous and heterogeneous oxidation with a characteristic lifetime of one to two days (Langner & Rodhe, 1991; Wojcik & Chang, 1997) to form sulfuric acid (H_2SO_4) and sulfate (SO_4^{2-}), therefore, contributing to new particle formation (Sipila et al., 2010) as well as the acidity of precipitation (Hegg & Hobbs, 1981) and aerosols (Weber et al., 2016). SO_2 as well has been measured extensively by mass spectrometry (Huey et al., 1995, 2004; Jurkat et al., 2010; Kim et al., 2007; Miake-Lye et al., 1998; Mohler et al., 1992; Seeley et al., 1997; Slusher et al., 2004; Speidel et al., 2007; Thornton et al., 2002) but is most commonly measured utilizing fluorescence (Luke, 1997; Matsumi et al., 2005; Okabe et al., 1973; Rollins et al., 2016; Schwarz et al., 1974; Simeonsson et al., 2012).

We describe modifications implemented on the HRToF-CIMS to allow simultaneous detection of a suite of RHS and their isotopologues, SO_2, and reactive nitrogen precursors (e.g., N_2O_5) and co-products (e.g., HNO_3 and $ClNO_2$). The modifications include (i) continuous humidification of the ion-molecule reaction (IMR) region to minimize the influence of ambient water vapor pressure variations on overall instrument sensitivity; (ii) a moveable, computer-controlled sampling orifice to maintain constant mass flow-rate of ambient air into the IMR region over a range of altitudes; (iii) in-flight calibration and characterization of sampling inlet effects by continuous addition of isotopically labeled ^{15}N dinitrogen pentoxide ($^{15}N_2O_5$); and (iv) frequent instrument background determinations by addition of ultrahigh purity (UHP)

N_2 to better account for the smearing due to rapidly occurring, short-lived plume encounters containing concentrated semi- to low-volatile compounds such as nitric acid (HNO_3). We evaluate the dependences of HCl and SO_2 measurements on water vapor pressure and compare to those of the other RHS and inorganic trace gases detailed elsewhere (Kercher et al., 2009; Lee et al., 2014). In-flight observations are shown from the Wintertime INvestigation of Transport, Emissions and Reactivity (WINTER) experiment (Guo et al., 2016), which utilized the highly instrumented NCAR-NSF C-130 aircraft based out of Norfolk, VA. In total, 13 research flights were performed achieving a total of 94.4 research flight (RF) hours. We present case studies from the WINTER experiment that illustrate the performance of the HRToF-CIMS in the context of the above modifications and that give insights into emissions and budget analyses provided by robust, simultaneous measurements of a large suite of compounds with the same instrument.

2. Instrument Description

Detailed descriptions of the Tofwerk AG HRToF-MS that is the core of the UW HRToF-CIMS instrument, including the vacuum chamber, ion optics, and data acquisition, are provided in previous publications (Junninen et al., 2010; Lee et al., 2014; Yatavelli et al., 2012). For the WINTER 2015 aircraft campaign, we reconfigured the instrument described in Lee et al. (2014) to fit within a 21 inches (53 cm) wide × 50 inches (127 cm) tall × 28 inches (71 cm) deep aircraft rack. The rack, excluding an online N_2O_5 calibration source, weighs 330 lb (150 kg) and draws 0.8 kW of power.

2.1. Aircraft Inlet and Sampling

To reduce losses and artifact generation during transfer of ambient air to the instrument, we employed a short residence time, atmospheric pressure inlet. The cross section of the inlet assembly was as shown in Figure 1a. Ambient air is drawn through a 40-cm-long, 1.9-cm outer diameter (OD), 1.6-cm inner diameter (ID) polytetrafluoroethylene (PTFE) tubing oriented orthogonal to the direction of flight. Approximately 18 cm of the inlet was housed in a streamline-shaped winglet attached to a custom-built window plate mounted on the wall of the aircraft. An additional 2.5 cm of inlet with a rear facing 45° cut—to reduce by inertial separation the amount of particles sampled—extended beyond the winglet end cap. We assume a constant volumetric flow-rate of 20 liters per minute through the sampling inlet was maintained—independent of altitude changes from sea level up to the maximum altitude encountered during WINTER of about 5 km above sea level—given the specifications of the pump dedicated to the inlet flow (Vaccubrand MD1). This translates to ~0.22-s mean residence time in the inlet. Of the total flow-rate entering the inlet, 2 slpm is subsampled from the centerline into the IMR region of the HRToF-CIMS through a 1.5-cm-long, 0.32-cm OD extruded PTFE tubing pressed into a computer-controlled variable orifice. The remaining flow is pumped radially through a circular slot located between the inlet and IMR entrance to minimize sampling of air that has been in contact with the inlet walls.

Heating the exterior of an inlet can improve response times (by minimizing adsorption), maintain constant sampling conditions, and therefore improve backgrounds. A disadvantage, however, is that the heating disrupts the equilibrium that exists between the semivolatile gas and particles, as well as potentially causing thermal decomposition of some gases such as N_2O_5 or peroxy nitrates. During wintertime experiments, the potential for perturbation is even greater given the significantly colder ambient air (~0 °C) compared to typical cabin temperatures or typical inlet heating regimes (25–80 °C). Therefore, the inlet to the HRToF-CIMS during WINTER was insulated on the inboard side of the aircraft such that the high flow-rate and slow heat transfer across the PTFE inlet kept incoming air at near ambient temperature. As the inlet was oriented orthogonal to the direction of flight with a 45° rear facing cut, we assume that the temperature perturbation due to ram heating had a negligible effect on measurements. The IMR region, likewise, was not temperature controlled but insulated. Though we applied no active heating, some temperature change likely occurred during the transfer of ambient air to the instrument. Neither the surface temperature of the inlet or IMR nor the air temperatures therein were measured during flight. Continuous addition of isotopically labeled formic acid ($H^{13}COOH$) to the entrance of a similarly designed inlet on a previous aircraft deployment (Lee et al., 2014) did not show significant loss of calibrant with altitude changes. However, the influence of changes in pressure and humiditiy on inlet transmission of a wider array of compounds still needs to be determined.

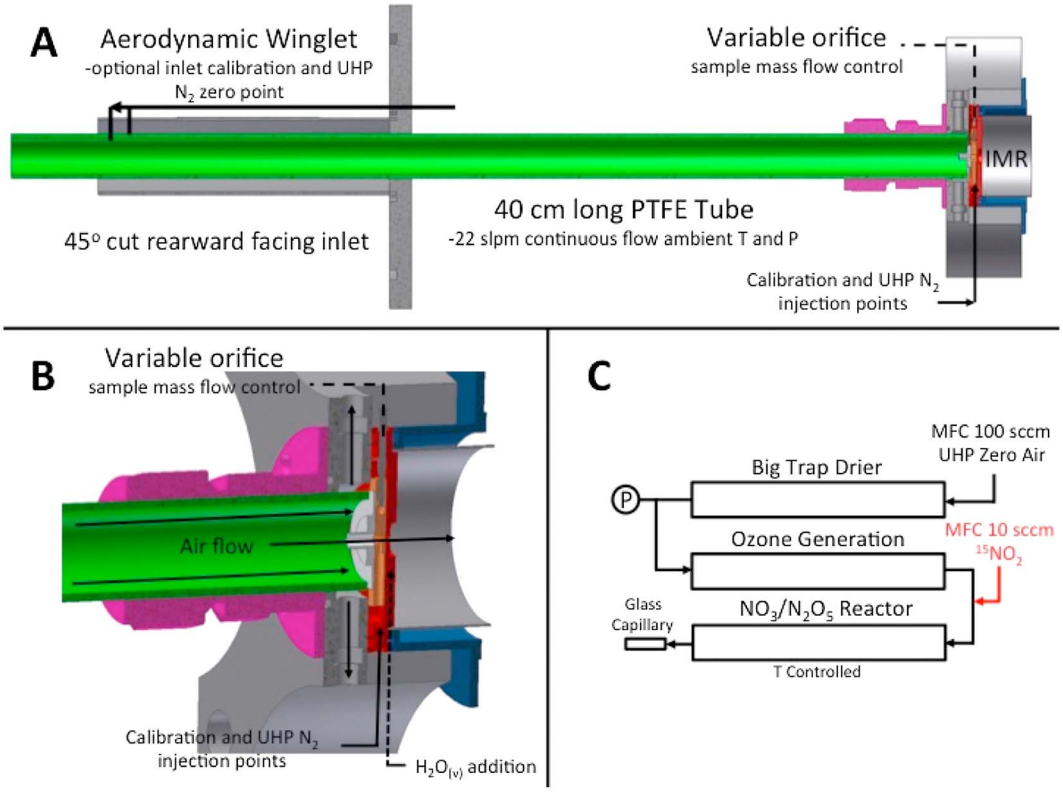

Figure 1. (a) Cross section of the 40-cm-long, 1.9-cm OD PTFE aircraft inlet designed to couple to the University of Washington high-resolution time-of-flight chemical ionization mass spectrometer (HRToF-CIMS) for the WINTER experiment. (b) A computer-controlled PTFE plate (orange color) slides dynamically with changing ambient pressure to act as a "variable orifice" to maintain constant mass flow-rate into the IMR region. Calibration and zero gases are introduced through a secondary pinhole that is orthogonal, on the sliding PTFE plate, to the pinhole through which ambient air enters the IMR region. (c) Schematic of the flight deployable calibration source that generates isotopically labeled $^{15}N_2O_5$. The source is taken off the aircraft after each flight to keep the internal components of the calibration system dry.

The IMR region was composed of a double-walled stainless-steel tube. The inner wall, treated with a hydrophobic Flouropel coating, is thinner than the outer wall to allow its body temperature to quickly equilibrate to the rapid temperature variations of the incoming air. The thicker outer wall, which without the inner wall would act as a heat sink, provides only structural support and does not interact with the ambient matrix.

2.1.1. Mass Flow and Pressure Control

Large-altitude variations encountered during research flights can lead to changes in internal pressures that affect response and ion molecule reaction times, both of which affect sensitivity. To address this issue, we fabricated and deployed an "iris" system to adjust the size of the IMR sampling orifice in response to changes in ambient pressure (altitude). The operating principle of this system is similar to that described by Crounse et al. (2006). A stainless-steel (bottom) and PTFE (top) plate, both with pinholes drilled through the center, were stacked in series to act as the IMR sampling orifice. The stainless-steel plate (Figure 1b, red) was fixed in place and had a slot in which the top PTFE plate (Figure 1b, orange) could slide relative to the stainless-steel plate. When perfectly overlapped, the two pinholes allow the maximum flow into the IMR region. The target flow-rate (2 slpm) into the IMR is obtained by moving the position of the PTFE plate, thereby altering the size of the effective pinhole. The total mass flow-rate through the IMR region is measured (MKS 179c) at the exit of the pump (Agilent IDP3), which is dedicated to pumping the IMR region. Another mass flow controller regulates the 2 slpm flow of UHP N_2—enriched with methyl iodide by a permeation device—introduced through the ion source (^{210}Po, 10 mCi, NRD) into the IMR region, and the flow drawn into the mass spectrometer is regulated by a critical orifice. The flow through the IMR region is monitored by the instrument operating system (LabVIEW) and a custom algorithm adjusts the absolute position of the

PTFE plate as well as the rate of adjustment via a microstepping stepper motor (Sanyo) connected to a stainless-steel threaded rod.

This iris system works in parallel with a custom servo-controlled valve (Swagelok), which throttles the IMR pump to maintain a constant pressure of ~75 torr in the IMR region, resulting in a mean residence time of ~30 ms. The pressure controller and variable pinhole also communicate via instrument control software to avoid overcorrections or cross-talk during rapid altitude changes. The orifice motion control always takes priority, as the sample flow directly affects pressure, and pumping speed changes are typically on slower timescales than aircraft ascents and descents. The 1σ variability of 94.4 flight hours of 1-Hz observations of the mass flow-rate into the IMR region and pressure in the IMR region were 73 sccm (2.1%) and 3.5 torr (4.9%), respectively. Altitude and mass flow-rate of ambient air into the IMR region during a WINTER RF is shown in Figure S1.

2.1.2. Water Vapor Control

The sensitivity of iodide-adduct ionization to many compounds is influenced by the absolute water vapor concentration in the IMR region, often changing rapidly near dry conditions, and more gradually under humid conditions (Kercher et al., 2009; Lee et al., 2014). This effect is most problematic when assessing instrumental backgrounds (discussed below) using dry UHP N_2 since the sensitivity between ambient and background determinations will change. Moreover, large variations in ambient humidity were expected for the campaign study area which included the cold continental boundary layer and the warmer marine boundary layer. To reduce the effects of ambient humidity variations and of changes between the ambient and background determinations, a 100-sccm flow of UHP N_2 saturated in water vapor was continuously added to the IMR region, resulting in at least 0.15 torr of water vapor pressure (comparable to measuring ambient RH of ~15% and ~60% RH at 0 °C and 20 °C, respectively) in the IMR at all times.

More tests are needed, however, to determine the effects of species present in ambient air but absent in UHP N_2 (e.g., oxygen, ozone, and carbon dioxide) on the iodide-adduct ionization sensitivity to the compounds presented. An ideal background gas would have the same composition as ambient air, except for the compounds of interest that would be absent. However, the suite of compounds simultaneously detectable with the HRToF-CIMS makes such a source of clean air somewhat ill-defined if there is cross-talk between different gases detected by the ion chemistry. Moreover, most zero-air generators would add weight and power to the payload given that UHP N_2 is required for the generation of iodide ions.

2.2. Calibration and Artifact Determinations

A custom-designed continuous-flow N_2O_5 source was built for calibration both in-flight and on the ground. The source mixes 2 sccm of ^{15}N nitrogen dioxide ($^{15}NO_2 > 99\%$; 10 ppm; Scott-Marin) with 100 sccm of UHP zero air (Air Liquide) containing concentrated ozone (O_3) generated by exposing the zero air to 185 nm radiation from a mercury lamp (PenRay). The mixture reacts in a 0.4-cm OD, 40-cm-long PTFE tubing before exiting through a 10-cm-long glass capillary (Accu Glass) used to maintain the gases in the generation system above 25 psig (Figure 1c) so as to minimize variations in the mass flow-rate, mixing ratios, and residence times in the reaction cell with changes in ambient pressure. The UHP zero air is initially passed through a 50-cm-long chemical drier (Chromatography Research Supplies) to minimize water penetration, and therefore, nitric acid ($H^{15}NO_3$) production from reaction of $^{15}N_2O_5$ on the reactor walls. The generation system was continuously operated to minimize transient effects since power was unavailable on the aircraft overnight. An uninterruptable power supply (5S1500 Eaton) allowed operation during transfer to and from the aircraft. The system, consisting of the $^{15}NO_2$ cylinder, UV source, reaction cell, and drier, weighs 17 kg and fits inside a half wide 4 U rack.

The output of the $^{15}N_2O_5$ generation system was verified utilizing two independently-calibrated total nitrogen oxide (NO_y) instruments (National Oceanic and Atmospheric Administration Cavity Ring-down Spectroscopy, NOAA CRDS; Wagner et al., 2011; Wild et al., 2014; and University of California Berkeley thermal dissociation laser-induced fluorescence, TD-LIF; Day et al., 2002; Wooldridge et al., 2010), which agreed to within 1.3%, well within the uncertainties of each technique. The $^{15}N_2O_5$ was periodically converted to nitryl chloride ($Cl^{15}NO_2$) using a wetted salt bed (Kercher et al., 2009; Lopez-Hilfiker et al., 2012). The resulting sample containing $Cl^{15}NO_2$, $H^{15}NO_3$, and $^{15}N_2O_5$ was measured by the HRToF-CIMS and quantified as a sum by the two NO_y instruments. The difference between NO_y and the sum of $H^{15}NO_3$ and $2\times^{15}N_2O_5$—both

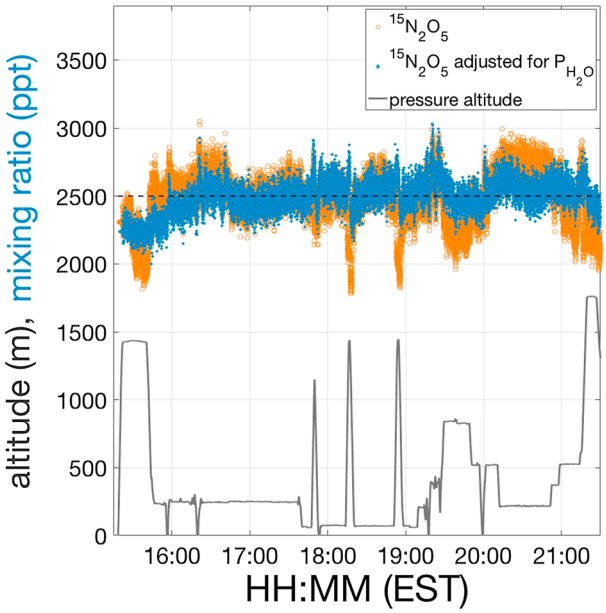

Figure 2. Mixing ratio of $^{15}N_2O_5$ (delivered continuously from the flight calibration source) and altitude during RF01 (February 3). The apparent decrease in $^{15}N_2O_5$ mixing ratio (gold, obtained by applying the flight-median sensitivity of N_2O_5) with increasing altitude demonstrates the effect of changing water vapor pressure on instrument sensitivity. This effect is accounted for those species for which the sensitivities dependence on water vapor pressure is known, as shown here for $^{15}N_2O_5$ (blue, obtained by applying sensitivity adjusted given the variability in the water vapor pressure in the IMR region).

quantified by the HRToF-CIMS—allowed $Cl^{15}NO_2$ quantification; thus, the coupled systems provided a calibration for both N_2O_5 and $ClNO_2$. Sensitivity to HNO_3 was also verified during WINTER by introducing HNO_3 to the University of California Berkeley TD-LIF instrument, as well as NCAR's NO/NO_y instrument that quantitatively converts HNO_3 by heated gold catalyst followed by measurement of NO via chemiluminescence (Ridley et al., 2004).

To establish in-flight stability of the HRToF-CIMS employing the sampling procedure described above, we continuously added isotopically labeled dinitrogen pentoxide ($^{15}N_2O_5$) through a 0.16-cm OD PTFE tubing just upstream of the pinhole leading to the IMR region for the duration of three test-flights and the first research flight (RF01). The combined effects of instrument detection efficiency and calibration source output were stable to within 20% across the entire RF01 (median ± standard deviation = 2.5 ± 0.12 ppb), as shown in Figure 2. Continuous $^{15}N_2O_5$ addition was not conducted for the remaining research flights to improve observations of SO_2, which is detected at the same nominal *m/z* as $H^{15}NO_3$ (discussed below).

The Reynolds numbers for the inlet flow near sea level, 0.7 km (WINTER median) and 5 km (WINTER maximum), were 2,000, 1,700 and 1,000, respectively. Though calculations indicate that the average flow in the inlet is close to laminar, we assume the flow to be turbulent at the inlet tip given the instability introduced at the rear-facing cut at its entrance but approaches laminar flow within five diameter-lengths, that is, within 8 cm from the entrance of a 40-cm-long inlet (Kay & Nedderman, 1974). To determine the extent to which the inlet was a source or sink of reactive trace gases, we introduced $^{15}N_2O_5$ via a 0.16-cm OD PTFE tubing orthogonal to the main flow located approximately 5 cm downstream of the inlet entrance before and after a RF to determine if any residue on the inlet induced loss or artifact formation. Adding $^{15}N_2O_5$ to the inlet before or after a RF yielded upward of 1 ppt $ClNO_2$ per 100 ppt of N_2O_5 added (Figure S2; median $ClNO_2/(N_2O_5 + ClNO_2) = 0.0045$), due presumably to conversion on instrument surface, with negligible lingering effects. During most WINTER periods, the observed level of $ClNO_2$ far exceeded the amount potentially formed due to instrument surface conversion assuming a 1:100 N_2O_5:$ClNO_2$ conversion ratio (Figure S3). However, a more thorough assessment must be conducted during periods of low $ClNO_2$ and high N_2O_5 (Figure S3). Addition of $^{15}N_2O_5$ to the inlet—as opposed to just upstream of the IMR entrance—during flight was not conducted so the potential conversion on inlet surface under lower ambient pressure but turbulent flow at the inlet tip was not characterized.

In addition to the above N_2O_5 and $ClNO_2$ calibrations, we tested the instrument response to a range of other trace gases, including HNO_3, HCl, Cl_2, HOCl, HONO, HNCO, and SO_2, using a variety of methods before and after the WINTER campaign, while the instrument was in the same configuration. Br_2 and HNO_3 were calibrated using permeation devices whose output rates were verified by gravimetric analysis. HCl was calibrated using microinjections of solutions in methanol (Sigma-Aldrich) with known concentrations as described previously (Lee et al., 2014). HONO and HNCO were calibrated using sources verified by an NO_y detector (Wild et al., 2014). Sensitivities to Cl_2 and SO_2 were determined using compressed gas standards (10.1 ppm ± 5% SO_2 in N_2, Scott-Marin; 7.5 ppm ± 5% Cl_2 in N_2, Praxair). HOCl was calibrated by quantitatively converting to Cl_2 following the protocol described by Foster et al. (1999). Generating standards for HBr, $BrNO_2$, HOBr, and BrCl is not trivial (Barnett, 1988; Caloz et al., 1998; Foster et al., 2001; Orlando & Burkholder, 1995). As such, we scale the sensitivity of $BrNO_2$ obtained from quantum chemical calculations (Iyer et al., 2016) by the ratio of the observed to calculated sensitivity of their chlorine counterpart. For BrCl, we apply the mean of the sensitivities of Cl_2 and Br_2 to obtain 2.5 ncps/ppt, which is comparable to the sensitivity obtained by quantum chemical calculations of 3.0 ncps/ppt (Table S1). Unlike for HNO_3 and SO_2, no other instrument existed to which the HRToF-CIMS measurements of halogen containing

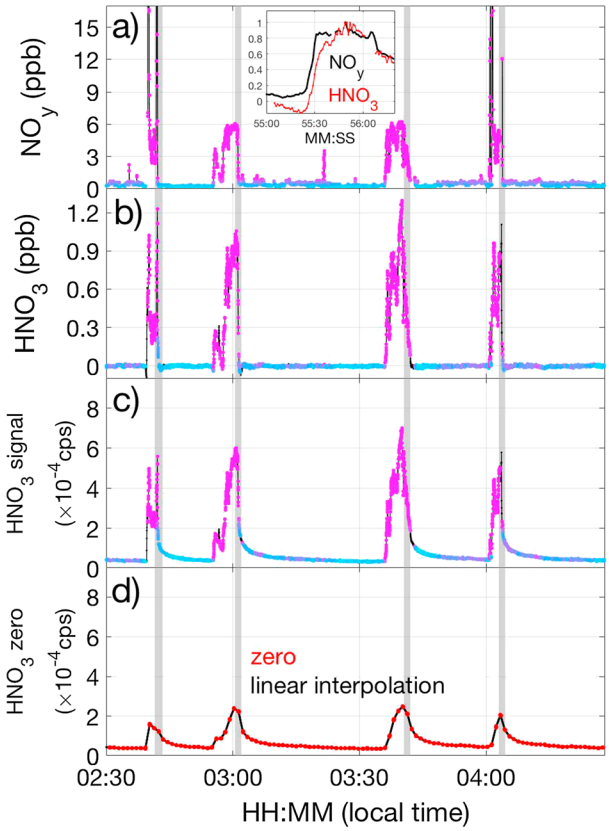

Figure 3. (a) NO_y mixing ratio measured by NOAA CRDS, (b) HNO_3 mixing ratio by HRToF-CIMS, and (c) HNO_3 signals during ambient measurements, and (d) background determinations (see text for details on frequency and duration). The mixing ratio reported in (b) is the difference between (c) and (d) followed by applying water vapor pressure and total reagent ion count rate adjusted sensitivities. Note the long tail in (c) following prolonged encounters of air mass containing high HNO_3 levels that is not evident in (a) NO_y. Accounting for instrument surface memory effects with frequent background determinations as seen in (d) results in HNO_3 response times that are more consistent with that of NO_y. Without frequent background determinations (red markers in panel d), such memory effects cannot be accounted for. Traces in (a), (b) and (c) are colored by NO_y mixing ratio for visualization of the memory effects. Markers above 1 ppb NO_y are magenta, cyan for those below 1 ppb, and are connected by black lines. The shaded gray vertical lines help visualize the improvement in HNO_3 response times with frequent background determinations. The inset shows normalized NO_y and HNO_3 mixing ratios during the beginning of the plume encounter occurring just before 3 am (local time). The level of HNO_3, normalized to its local maximum during this period, plateaus on the timescale of several seconds, comparable to that of NO_y, as the aircraft transitions from sampling a clean to a polluted air mass.

compounds could be compared. As such, we rely on the accuracy of our traceable calibration standards for these compounds.

Instrument sensitivities to HCl and SO_2 decrease with increasing water vapor pressure in the IMR region (Figure S4), whereas those to HNO_3, N_2O_5, Cl_2, Br_2, and $ClNO_2$ increase (Kercher et al., 2009). The sensitivities to the species reported here vary by less than 20% over the range of water vapor pressures in the IMR region encountered during WINTER (Figure S3) owing to the continuous addition of humidified UHP N_2. Corrections are, nonetheless, applied to account for this variability to obtain final mixing ratios. No water vapor dependence corrections, however, were made to HOCl, and $BrNO_2$.

2.3. Background Determinations and Detection Limits

Instrument (IMR) background signal determinations were conducted in-flight every 60 s for a duration of 5 s by flowing UHP N_2 through a 3.2-mm OD port built into the moveable PTFE plate at a flow-rate exceeding that entering the IMR region. Overall background signal determinations, representing the sum of inlet and instrument (IMR), were also performed by overflowing from the entrance of the inlet with a high flow-rate (>30 lpm) of UHP N_2 for 10 s on several occasions during the first few research flights. For IMR backgrounds, the UHP N_2 enters at the pinhole perpendicular to the flow going into the IMR region to displace the incoming ambient air (Figure 1b). Typically, the first and last two 2-Hz data points of the 5-s zero mode are discarded to avoid incorporating transitional signal in the average, and the remaining points are used to characterize the instrument background for each high-resolution fit ion peak (Figure S5). Each of these backgrounds determined every 60 s are then linearly interpolated to the ambient sampling time-base for subtraction from the signal measured during ambient air sampling.

The guiding principle to this approach is that for "sticky" or semi- to low-volatility compounds, the background signal most often results from evaporation of the compounds adsorbed to IMR or inlet surfaces or present in particles deposited on these surfaces. The evaporation flux from these surfaces will depend upon surface coverage, which will reflect a balance between the concentration-dependent transport of trace gases or particles from the sample flow to the walls. Importantly, the flux from surfaces will decrease as surface coverage decreases or when the concentration in the sample air decreases, such as during a background determination or when transiting from polluted air to clean air. Therefore, the shortest determination of the signal in clean air (or N_2) will provide the truest measure of the instrumental background that results from this desorption flux. Longer sampling of clean air will lead to systematically lower estimates of the background concentration as the flux from surfaces will decrease. The timescale over which such a decrease occurs will depend upon the specific compound, the surface area exposed to sample air, dead volumes, and exchange rates. We found 5-s UHP N_2 additions to be a reasonable balance between minimizing perturbation to the inlet and instrument surfaces, which are forced out of (pseudo) equilibrium during the background determinations, and obtaining sufficient points for a statistically representative background determination (Figure S5). For the RHS and SO_2 that are a foci of this work, lingering or residual background signal following encounters of concentrated air parcels are less of an issue given their lower Henry's law constants compared to that for nitric acid.

This background approach does not address underestimates of ambient concentrations, which might occur when transitioning from a clean environment, where instrument surfaces are not close to saturation, to a

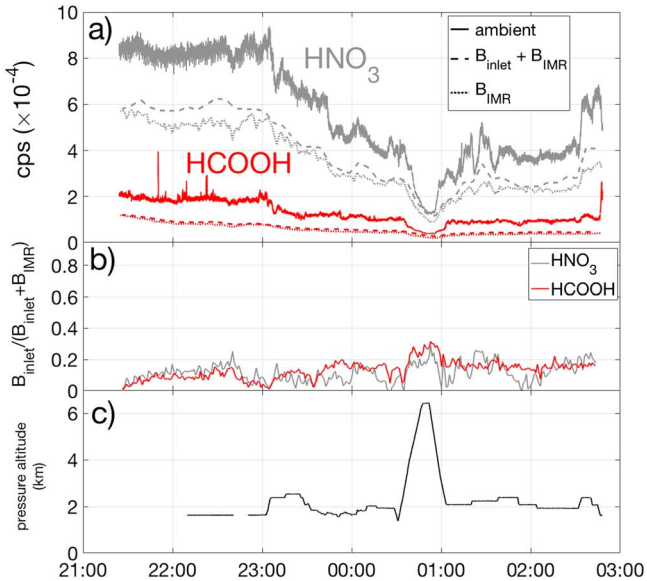

Figure 4. (a) Ambient signal (solid), total background signal due to the inlet and IMR region (dashed: $B_{inlet} + B_{IMR}$), and background signal due to the IMR region only (dotted: B_{IMR}) are shown for (gray) nitric acid and (red) formic acid. (b) Fraction of the background signal due to the inlet relative to total, $B_{inlet}/(B_{inlet} + B_{IMR})$. (c) Pressure altitude in km. The median ± standard deviation of background signal contribution from the inlet relative to the total for HNO_3 and HCOOH is 0.11 ± 0.06 and 0.14 ± 0.06, respectively. Elevated $B_{inlet}/(B_{inlet} + B_{IMR})$ are associated with periods of low ambient and background signal levels, such as at high altitude.

more polluted environment (e.g., from above the boundary layer into it). In this case, a trace gas that partitions to available surface area will be net removed from the sample stream leading to a lower signal and thus a low bias in the reported concentration. Utilizing small exposed surface areas and high exchange rates facilitates more rapid approach to saturation. Overall this issue is likely less pervasive a problem, except in spatially narrow plumes, as the approach to saturation is governed by turbulent mixing of air to the IMR walls (in our system) while the evaporation timescale is likely much longer, being governed by the strength of the interaction between the compound and wall surface. For example, during calibrations or when transitioning from a clean to a polluted region, the signal for HNO_3 typically reaches ~90% of its steady state value within a few seconds when accounting for the IMR background changes that occur with the pulse of external HNO_3 (Figure 3).

For most species detected by the HRToF-CIMS, the backgrounds generally exhibit a double exponential decay following a concentrated pulse (Figure S5). The first decay portion is fast, consistent with the residence time in the IMR (one *e*-fold residence time ~30 ms at 80 torr). The second decay can be slower due likely to interaction with the stainless-steel IMR surfaces and turbulent flow in the IMR region downstream of the sampling orifice. Despite the short IMR residence time, the decay time of ambient signals for semi volatile gases, such as HNO_3, can be several seconds long following an encounter with air containing high concentrations (Figure 3c) due predominantly to the delayed contribution from residual material being released from the IMR surface as the aircraft transitions to a cleaner region (Figure 3d). The frequent but short instrument background determinations (Figure 3d) allowed these short-term fluctuations in IMR memory to be captured. Subtracting out the residual signal originating from the IMR surface (Figure 3d) from the ambient signal (Figure 3c) yield HNO_3 mixing ratios, which have a temporal behavior (Figure 3b) more similar to that of independently measured NO_y (Figure 3a).

Additionally, the overall background signals (inlet + IMR) were not significantly higher than those conducted at the entrance of the IMR region (Figure 4), indicating that memory effects are largely from the surface of the IMR region compared to the inlet where the large volumetric flow dilutes off-gassing. Thus, the 40-cm-long PTFE inlet was typically a minor contributor compared to the IMR region to the total residual background signal for most species measured during WINTER. The inlet configuration presented here represents our best approach at minimizing residence time and turbulence while utilizing an inlet with a diameter large enough to subsample the centerline flow that is less influenced by its surface. Such an approach showed background signal contribution from the inlet that was much lower compared to that originating from the IMR region (Figure 4). Conversely, the inlet may contribute a greater amount to the overall background under different configurations or conditions.

The signal remaining at the end of each background determination reflects the amount of material evaporating from the IMR surfaces, along with, in the case of HNO_3, a relatively small and constant amount from the ^{210}Po ion source. A fraction of the background signal, which is typically approximately one third of the ambient signal, therefore represents vapor that had partitioned to the surfaces during transit through the IMR that went unmeasured. The remaining fraction is from other sources such as particles, which impacted and volatilize or the ion

Table 1
List of Polarizability (bohr^3), Sensitivities (ncps/ppt) and Limits of Detection

Species (formula)	Polarizability (bohr^3)	Sensitivity (ncps/ppt)	1-s 1-σ LOD (ppt)	10-s 1-σ LOD (ppt)
SO_2	26.65	0.028	160	48
HCl	17.92	0.03	82	22
Cl_2	31.36	2.9	0.4	0.1
$ClNO_2$	39.51	1.7	0.6	0.1
HOCl	23.41	0.5	4	1
Br_2	46.72	2.0	0.5	0.1
$BrNO_2$ †	48.35	1.7	1.0	0.3
BrCl	38.82	2.5	0.9	0.2
HNO_3	--	9.0	7.0	2.2
N_2O_5	--	6.6	0.4	0.1

Note. $BrNO_2$ sensitivity was obtained by scaling its calculated sensitivity (Iyer et al., 2016; Lopez-Hilfiker, Iyer, et al., 2016) by the ratio of the calculated to observed sensitivity of Br_2. The LOD value accounts for sensitivity of the compound as well as the variability in the amount of the compound encountered during background determinations throughout the WINTER campaign (Bertram et al., 2011)

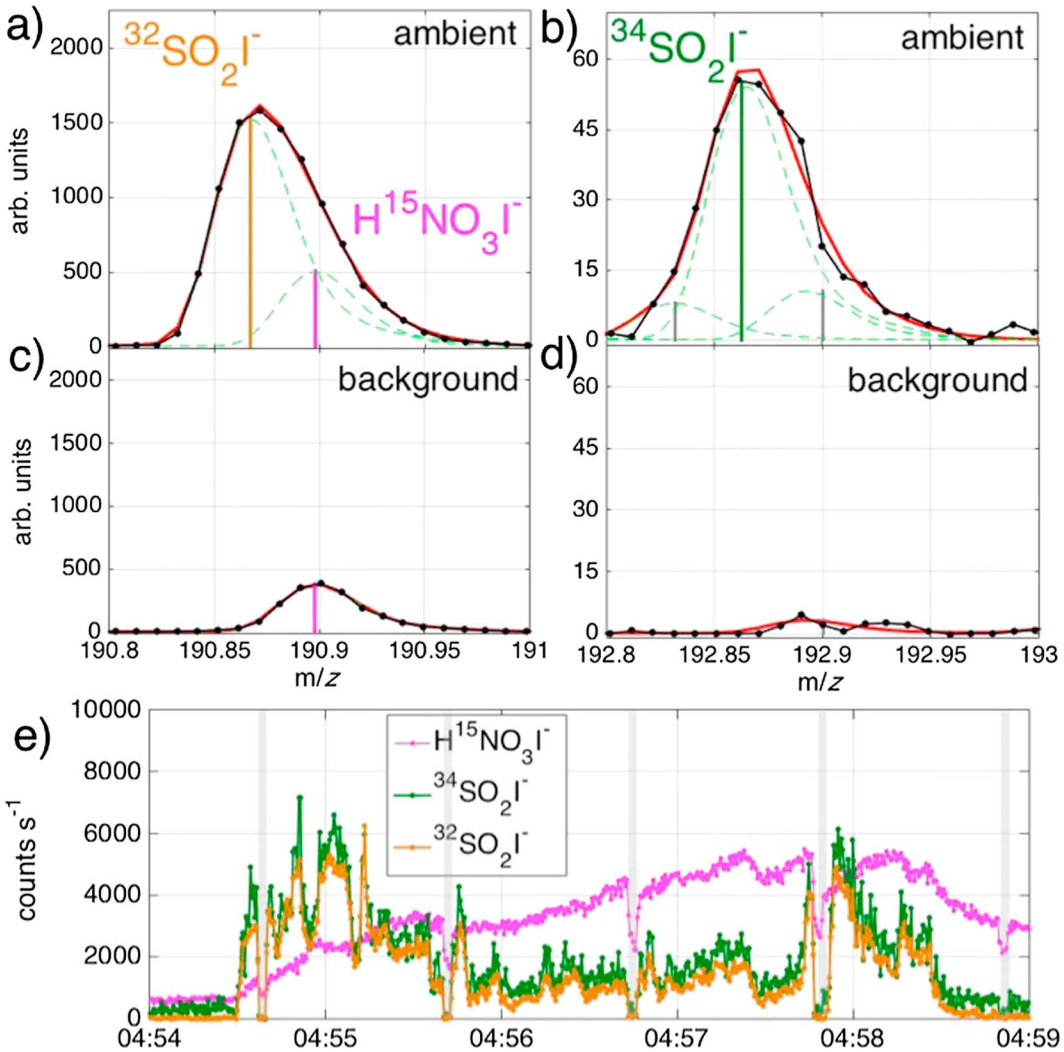

Figure 5. Spectra at nominal (a) *m/z* 191 Th and (b) *m/z* 193 Th where $^{32}SO_2I^-$ and $^{34}SO_2I^-$ are observed, respectively, during encounter of air parcel containing 23 ppb of SO_2 on RF07 (February 24). The predicted signal strength and location of $^{34}SO_2I^-$ (green) given those of $^{32}SO_2I^-$ (gold) are consistent with the observed spectra (black) at *m/z* 192.8627 Th. (c and d) Corresponding spectra during instrument background determination when the IMR region is flooded with UHP N_2 displacing ambient air are shown. (e) Time series of $^{32}SO_2I^-$, $^{34}SO_2I^-$, and $H^{15}NO_3I^-$ are shown. Though $H^{15}NO_3I^-$ appears at the same nominal *m/z* as $^{32}SO_2I^-$, the two are readily distinguished, as noted by their distinct behaviors in time (e). Formic acid clustered with iodide and water vapor $CH_2O_2H_2OI^-$ at *m/z* 190.9211 also does not affect measurement of $^{32}SO_2I^-$ as it occurs at a higher *m/z* than $H^{15}NO_3I^-$ and is typically observed at negligible levels. The signal of $^{34}SO_2I^-$ in (e) is scaled by the natural abundance of ^{34}S relative to that of ^{32}S to show its agreement with $^{32}SO_2I^-$.

source. The instantaneous amount of unmeasured vapor likely falls within our stated uncertainty (±30%), but the IMR surfaces may integrate the amount such that over time the background grows until an equilibrium is reached. Moreover, we conduct calibrations to HNO_3 and other trace gases in the same way ambient measurements are made, that is, by normalizing the signal difference between ambient and background by the known amount of material introduced. The resulting sensitivity accounts for the proportional loss to the surface of the IMR region.

Ideally, an instrument exhibits no memory effects. Our approach has been to balance reducing the extent of memory while still allowing sufficiently long interactions in the IMR region to achieve acceptable levels of sensitivities. Conducting frequent and short background determinations, while not the perfect solution (as discussed above), is one way to account for lingering signals following polluted air mass encounters.

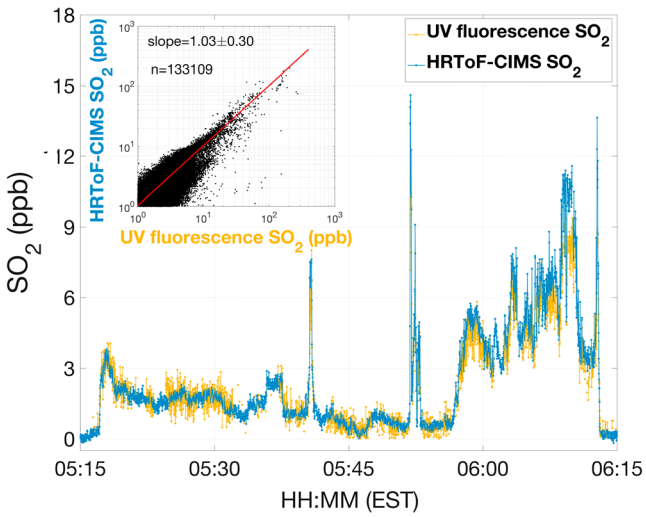

Figure 6. SO_2 mixing ratios as measured by HRToF-CIMS (blue) and UV fluorescence (gold) during RF07 (February 23). A potential NO artifact in the UV fluorescence technique is accounted for by assuming 25 NO molecules yield 1 molecule of SO_2 (Luke, 1997; Ryerson et al., 1998). The inset shows the intercomparison for WINTER when there is data overlap between the two SO_2 techniques and NO measured by NOAA CRDS (n = 133109 1-Hz data points). The lower limit on the inset is 1 ppb to reflect the 1-σ1-s precision of the UV fluorescence technique. The two techniques generally agree well, exhibiting a slope of 1.03 ± 0.30. Cross-calibration between the two instruments using a common SO_2 source was not performed.

Given their large negative mass defects, the background noise for chlorine and bromine containing compounds are typically lower than those composed only of carbon, oxygen, and hydrogen atoms. Their limits of detection, therefore, are mainly a function of their sensitivity to iodide-adduct ionization and detector noise. Compounds such as SO_2, HCl, and HOCl form weaker clusters with the iodide reagent ion compared to Cl_2, Br_2, $BrNO_2$, and $ClNO_2$, possibly related to the lower polarizabilities of the former compounds compared to the latter (Table 1). Additionally, HBr and HOBr are detected at the same nominal masses as two sulfur containing ions, SO_3I^- and SO_4I^-, respectively, that are detected in high abundance in coal-fired PP plumes. As such, HBr and HOBr were not positively identified in these plumes containing high levels of sulfur oxides. The $^{81}BrI^-$ (m/z = 207.8213 Th) ion, as well, exhibits high signal relative to and at the same nominal mass as $ClNO_2I^-$ (m/z = 207.8668 Th) within coal-fired PP plumes, but the two different ions are easily distinguished with the current mass resolving power of the instrument.

WINTER-mean sensitivities and limits of detection for the species of interest are listed in Table 1. Ultimately, a limit of detection is a function of both sensitivity and background level, neither of which is a constant. Sensitivity varies mainly as a function of variability in water vapor pressure, the effect of which is lowered by the humidification of the IMR region. Variability in background levels is driven primarily by encounters of polluted air parcels, as seen in Figure 3. More frequent encounters of concentrated events result in higher and more variable background levels, hence, higher limits of detection. The estimated uncertainty is 30% for species that were directly calibrated, including HNO_3, N_2O_5, Br_2, Cl_2, HOCl, $ClNO_2$, HCl, and SO_2. Based on scatter about the relationship between calculated and measured sensitivities, the uncertainty is around 50% for those species whose sensitivities we rely on calculations, including $BrNO_2$ and BrCl.

3. SO_2 Detection by CIMS and Measurement Comparison

During the WINTER 2015 experiment, SO_2 was measured by the UV fluorescence technique (Ryerson et al., 1998) and by the HRToF-CIMS instrument as SO_2 clustered with the iodide reagent ion at m/z 190.8669 Th, as first demonstrated by Friedman et al. (2016) in laboratory chamber studies. We therefore used the WINTER campaign to verify the HRToF-CIMS method by comparison to the well-established UV fluorescence technique.

Sulfur possesses a minor stable isotope (^{34}S) heavier by 2 amu with nonnegligible natural abundance (~4.3%). A sample mass spectra of $(^{32}SO_2)I^-$ and its most abundant minor stable isotope $(^{34}SO_2)I^-$ recorded during a WINTER RF are shown in Figure 5. The signal locations at m/z 190.8669 Th and 192.827 Th as well as the relative strengths of signal enhancements given the natural abundances of ^{32}S and ^{34}S are consistent with $(^{32}SO_2)I^-$ and $(^{34}SO_2)I^-$. Their retrieved signals, which are 2 amu units apart, are correlated well in time (Figure 5e). SO_2 measured by the two techniques agreed to within the uncertainty of the HRToF-CIMS, exhibiting a slope of 1.03 ± 0.30 and correlation coefficient (R^2) of 0.83 accounting for 133109 1-Hz data points (Figure 6), supporting that the measurement by the HRToF-CIMS at m/z 190.8669 Th is indeed SO_2 and that the calibration of the CIMS is well constrained during the campaign even though in-field calibrations were not conducted for SO_2. The UV fluorescence measurement was adjusted for potential interference from NO by assuming 25 molecules of NO yields 1 SO_2 molecule (Luke, 1997; Ryerson et al., 1998).

A limit of detection (LOD = 1-s 1σ) for SO_2 of 42 ppt was achieved for the HRToF-CIMS in the laboratory under dry conditions. During WINTER, the mean LOD accounting for all 13 research flights was around 160 ppt, compared to about 1 ppb for the UV fluorescence technique (Ryerson et al., 1998). The presence of $H^{15}NO_3I^-$ at nominal m/z 191 from the addition of isotopically labeled $^{15}N_2O_5$ was the biggest contributor of SO_2

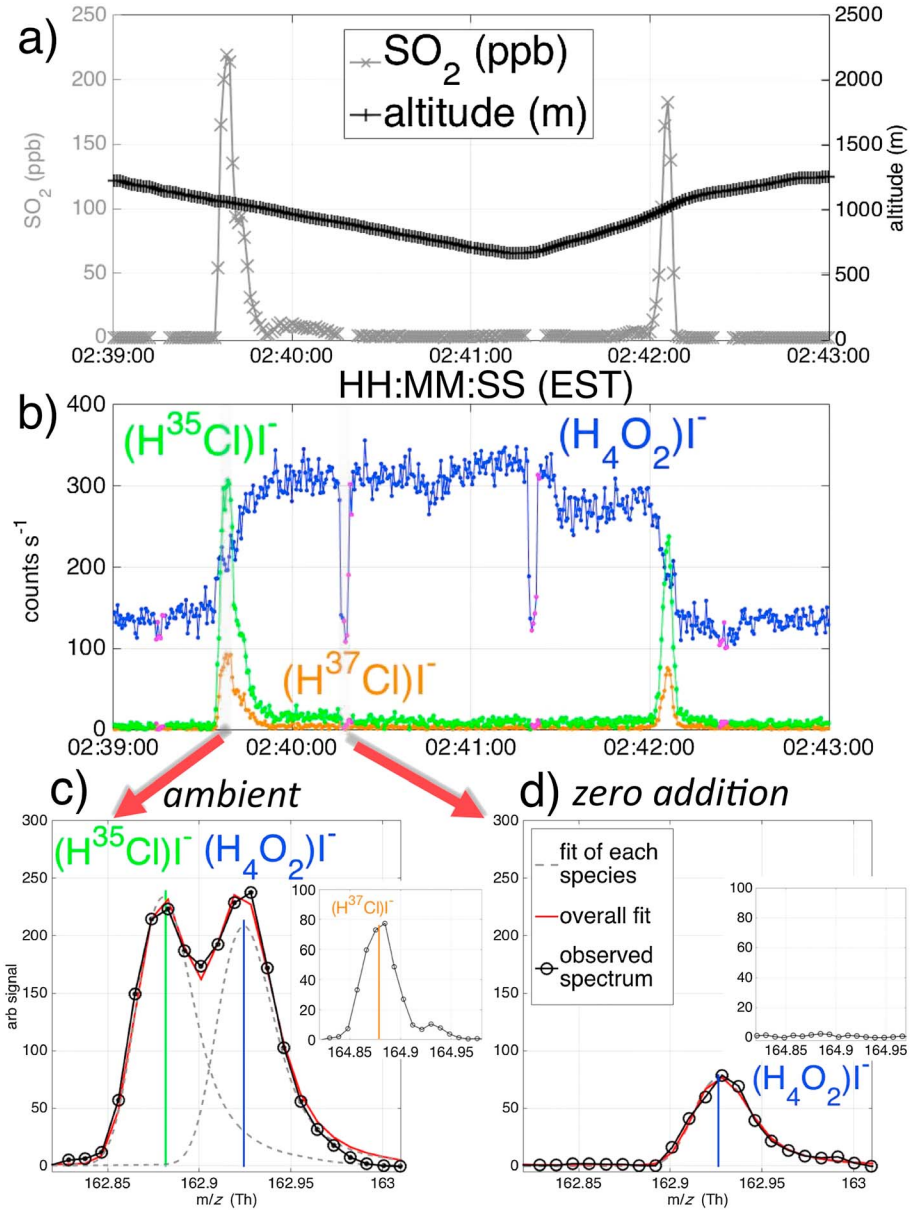

Figure 7. (a) SO_2 mixing ratio, altitude, and (b) signals of $H^{37}ClI^-$, $H^{35}ClI^-$ and $(H_2O)_2I^-$ during RF09 (3 March). (c) Spectrum at *m/z* 163 Th during the descent when levels of SO_2 (220 ppb) and HCl (10 ppb) were enhanced. (d) Spectrum at nominal *m/z* 163 Th during an instrument background determination, indicated by magenta markers in (b). Insets in (c) and (d) show corresponding spectra at *m/z* 165 Th where $H^{37}ClI^-$ is observed. The predicted signal strength and location of $H^{37}ClI^-$ (gold) given those of $H^{35}ClI^-$ (green) are consistent with the observed spectra (black) at *m/z* 165. Though $(H_2O)_2I^-$—reflecting the behavior of water vapor—appears at the same nominal *m/z* as $H^{35}ClI^-$, the two are readily distinguished, as noted by their distinct behaviors in time (b).

background noise. The approach described herein is suitable for detecting atmospheric SO_2 along with a suite of other organic and inorganic species with no modification to existing instrument protocol in regions with moderate to high levels of pollution.

4. Measuring Inorganic Chlorine and Bromine Containing Species

A suite of chlorine and bromine containing compounds including HCl, Cl_2, $ClNO_2$, HOCl, BrCl, Br_2, and $BrNO_2$ were observed during WINTER, in particular, at the emissions of coal-fired PPs. An example of a PP plume intercept is summarized in Figure 7. During this nighttime encounter over eastern Pennsylvania, PA, on

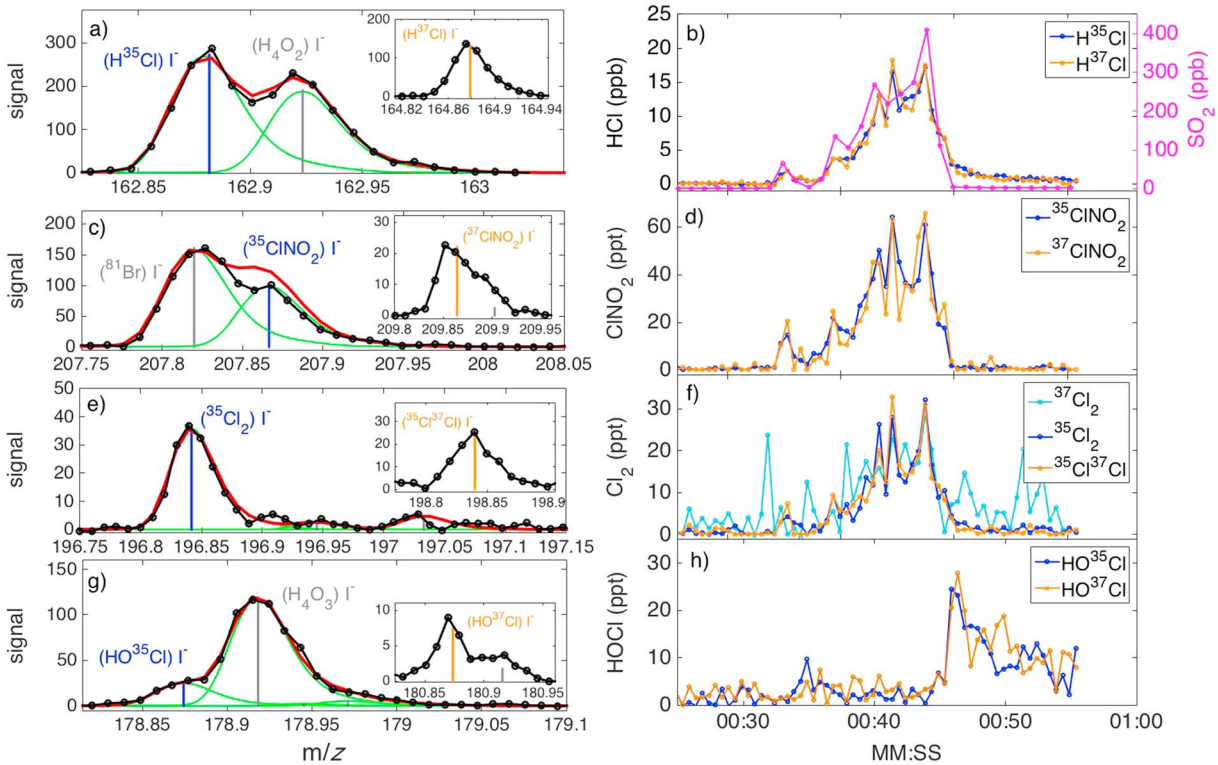

Figure 8. Spectra of (a) $HCl I^-$, (c) $ClNO_2I^-$, (e) Cl_2I^-, and (g) $HOCl I^-$ recorded at nominal *m/z* 163, 208, 197, and 179 Th, respectively, during RF11 (9 March). Insets show the corresponding spectra at *m/z* + 2 Th. (b, d, and f) The corresponding mixing ratios of the major and minor isotopes are well correlated with that of (b) SO_2 except that of (h) HOCl, which was enhanced outside of the main plume, suggesting a co-located but different emission source. Mixing ratios of the minor stable isotopes were obtained by applying the same sensitivities listed in Table 1 and scaled by the natural abundance of ^{37}Cl relative to ^{35}Cl.

RF9 (3 March), enhancement of SO_2 mixing ratios was observed during a descent followed by an ascent (Figure 7a). Distinct PP plumes during the descent/ascent portions of a profile but not at the nadir were commonly observed during nighttime flights when warmer exhaust from tall PP stacks resulted in a layer of pollutants residing above the cooler nocturnal surface layer. The HRToF-CIMS detects HCl clustered with iodide as $(HCl)I^-$ at mass-to-charge (*m/z*) 162.8817 Th. The iodide ion clustered with two water vapor molecules, $(H_2O)_2I^-$ (*m/z* 162.9262 Th), resides approximately 273 ppm ($10^6 \times \Delta m/z$/round [*m/z*]) from $(HCl)I^-$. The presence of $(H_4O_2)I^-$, even at artificially elevated water vapor pressures in the IMR, did not significantly affect the instrument's ability to detect $(HCl)I^-$. The two species (Figure 7) are easily distinguished given instrument spectral resolution (~5,000) and mass accuracy <20 ppm (Junninen et al., 2010; Lee et al., 2014; Yatavelli et al., 2012).

Carbon (^{12}C), nitrogen (^{14}N), and hydrogen (^{1}H) possess minor stable isotopes that are heavier by 1 amu (^{13}C, ^{15}N, and ^{2}H) and whose abundances are 1% or less of their major counterparts. Chlorine (^{35}Cl) and bromine (^{79}Br) possess minor stable isotopes that are heavier by 2 amu (^{37}Cl, ^{81}Br). ^{37}Cl is 32% and ^{81}Br is 98% of the abundances of their respective major isotope counterparts. The acquisition of the entire mass spectrum in a time-of-flight mass spectrometer means that the signal at every halogen isotopologue is measured nearly simultaneously, providing a strong constraint in halogen identification. The inset in Figure 7c shows a spectrum at nominal *m/z* 165 Th where the stable isotope $(H^{37}Cl)I^-$ resides. During PP plume encounters, signals for both $(H^{35}Cl)I^-$ at nominal mass 163 Th (Figure 7c) and $(H^{37}Cl)I^-$ at nominal mass 165 Th (Figure 7c inset) are enhanced. Signal at nominal mass 164 Th is unchanged (not pictured). The signal at nominal *m/z* 165 Th expected (Figure 7c inset: orange vertical bar) from that of $(H^{35}Cl)I^-$and the known abundance of ^{37}Cl relative to ^{35}Cl are consistent with the spectral location and strength of signal enhancement in the observed spectrum (Figure 7c inset: black markers). When ambient air is displaced by flooding the IMR with UHP N_2, signals of both $(H^{35}Cl)I^-$ and $(H^{37}Cl)I^-$ approach zero (Figure 7d). Accordingly, there is good agreement ($R^2 > 0.85$) in the retrieved time series for $(H^{35}Cl)I^-$ and $(H^{37}Cl)I^-$ (Figure 7b).

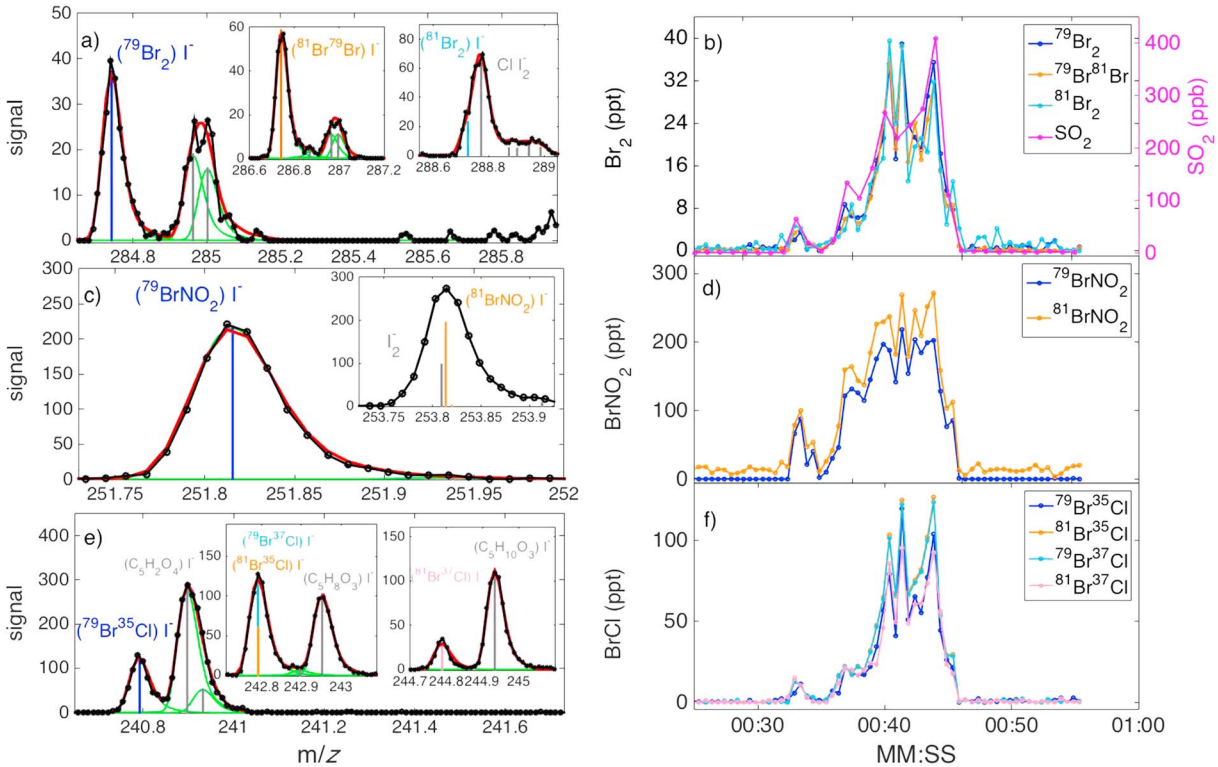

Figure 9. Same as Figure 8 but for (a) Br_2I^-, (c) $BrNO_2I^-$, and (e) $BrClI^-$. Signal for Br_2 at nominal *m/z* 287, composed of both $^{79}Br^{81}Br$ and $^{81}Br^{79}Br$, is greater by roughly a factor 2 than that at *m/z* 285 Th, which is composed of just $^{79}Br^{79}Br$.

Another PP plume encounter—during which levels of Cl_2, $ClNO_2$, HOCl, Br_2, $BrNO_2$ and BrCl are all enhanced—provides an example of the utility of fast time-response, simultaneous and sensitive measurements afforded by the HRToF-CIMS (Figures 8 and 9). The location and strength of the signal enhancement at 2 amu units greater than the nominal *m/z* of the major isotopes are consistent with those of its minor isotopes (insets of Figures 8 and 9). Their signals in time are highly correlated though the minor isotopes exhibit more noise owing to their lower natural abundance. The exception is Br_2, for which higher signal level is observed at *m/z* 286.7396 Th by approximately a factor of 2 due to contribution from both $^{79}Br^{81}BrI^-$ and $^{81}Br^{79}BrI^-$ compared to *m/z* 284.7417 Th at which only $^{79}Br_2I^-$ contributes. Signal for HOCl was enhanced a few seconds following those of the other species suggesting a co-located but not identical source, possibly a cooling tower (Chang et al., 2002; Tanaka et al., 2003). Many of these RHS are not the only species present at their nominal mass-to-charge, as shown in Figures 8 and 9. A mass spectrometer with high spectral resolution is, therefore, necessary for robust identification and quantification. The PP plume shown in Figures 8 and 9 is typical in that high concentrations of many different compounds are encountered over a short time period ranging from a few seconds to minutes. The HRToF-CIMS can measure them simultaneously with sufficient response times to obtain an accurate assessment of emission ratios.

5. Reactive Nitrogen Budget Analysis

One of the goals of the WINTER 2015 campaign was to identify and quantify the species that comprise total reactive nitrogen oxides (=NO_y), particularly, under nighttime winter conditions. While a more comprehensive NO_y budget closure assessment from WINTER is ongoing, we show an example from RF8 to support the conclusion that changes to the sampling and zeroing have improved, or at least not degraded, the ability to simultaneously measure HNO_3, N_2O_5, and $ClNO_2$ under rapidly changing air composition. The sum of the measurements of HNO_3, $2\times N_2O_5$, and $ClNO_2$ accounted for all NO_z (=NO_y–NO–NO_2) species (slope of 1.17 ± 0.30), at least, to within the HRToF-CIMS uncertainty of 30% during RF8 (Figure 10). The quantity NO_y–NO was measured using a TD-LIF instrument—the instrument to which the HRToF-CIMS was most

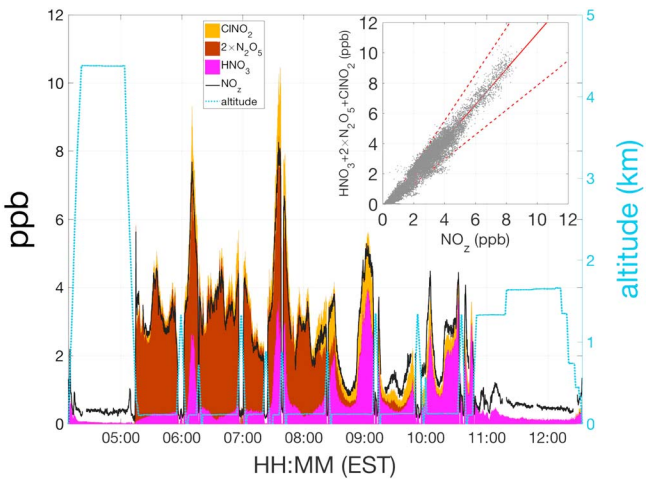

Figure 10. Mixing ratios of NO_z (=NO_y–NO_x), HNO_3, 2 × N_2O_5, and $ClNO_2$ during RF08 (march 1), along with altitude. The sum of HNO_3, 2 × N_2O_5, and $ClNO_2$ correlated well (R^2 = 0.96) with NO_z and explained all of NO_z to within the uncertainty of the HRToF-CIMS measurements during this morning to day transition flight off the coast of New York and New Jersey.

frequently calibrated in the field—by heating ambient air to 540 °C and subsequently measuring the resulting NO_2 formed as a result of thermal dissociation of nitrogen oxides, as well as the ambient NO_2 (Wooldridge et al., 2010). This temperature has been demonstrated to convert HNO_3, organic peroxy nitrates (ΣPNs), organic alkyl nitrates (ΣANs), $ClNO_2$, and N_2O_5 into NO_2, which is subsequently detected by LIF. NO is not measured by this technique since it is not converted to NO_2. Ambient NO_2 was also quantified by the TD-LIF through an unheated channel (Wooldridge et al., 2010). For this flight that occurred during the night-to-morning transition off the New York and New Jersey coast, a full accounting of the NO_z budget is achieved over a wide range of conditions as the C-130 flew in and out of distinct plumes influenced by urban outflow in the marine boundary layer. The missing NO_z at high altitudes is likely alkyl and peroxy nitrates (e.g., PAN), which the HRToF-CIMS did not calibrate for comparisons during WINTER. We chose this flight because it sampled polluted continental air that had mostly aged overnight. The HRToF-CIMS measures the NO_z components that are major products of nighttime NO_x chemistry (N_2O_5, $ClNO_2$, and HNO_3), and thus, the closure would be more sensitive to the calibration and transmission uncertainties associated with HNO_3 as discussed above. Given that HNO_3, N_2O_5, and $ClNO_2$ accounted for, at times, 57%, 92%, and 31% of NO_z, respectively, biases associated with inlet transmission and memory must be smaller than the associated calibration uncertainties. HONO does not thermally dissociate to NO_2, as such, is not measured by the TD-LIF technique. The median and 90th percentile HONO mixing ratios as observed by the HRToF-CIMS during this RF were 41 and 193 ppt, respectively. HONO, therefore, did not contribute significantly to the NO_z budget. A manuscript detailing a more comprehensive analysis of NO_y closure across all WINTER flights is in preparation.

6. Summary

We report on the upgrades implemented on the University of Washington flight-based HRToF-CIMS instrument employing iodide-adduct ionization. New features include (i) continuous addition of low-flow humidified UHP N_2 directly to the IMR region to minimize the difference in water vapor pressure, hence sensitivity, between ambient and background determinations; (ii) a dynamic pinhole that maintains a constant mass flow-rate into the IMR region independent of altitude changes to minimize variations in IMR region residence time; (iii) a portable system capable of constant addition of isotopically labeled $^{15}N_2O_5$ for in-flight calibration and overall instrument stability; and (iv) frequent but short-lived instrument zero determinations to account for surface memory effects to improve the response times to semivolatile gases. We demonstrate the utility of simultaneous and sensitive observations of a suite of compounds using observations from the WINTER 2015 flight experiment. Detection of a suite of halogen containing compounds in coal-fired PP plumes that are intercepted for brief durations and accounting for the reactive nitrogen budget by directly measuring each of the constituents is presented as examples. We also demonstrate the capability of measuring SO_2, HCl and a suite of other RHS by iodide-adduct ionization mass spectrometry.

Acknowledgments
The authors acknowledge the NSF-NCAR Research Aircraft Facility engineers, scientists, pilots, and staff members. Funding for J. A. T. was supported by the NSF AGS 1360745. J. C. S. , P. C. J., and J. L. J. were supported by NSF AGS-1360834. D. L. F. was supported by NSF AGS-1433358. E. L. D. was supported by NSF Graduate Research Fellowship under grant DGE-1256082. The WINTER observations presented here can be accessed on the NCAR/NSF website (http://data.eol.ucar.edu/master_list/?project=WINTER).

References

Arnold, S. T., & Viggiano, A. A. (2001). Turbulent ion flow tube study of the cluster-mediated reactions of SF_6^- with H_2O, CH_3OH, and C_2H_5OH from 50 to 500 torr. *The Journal of Physical Chemistry. A*, *105*(14), 3527–3531. https://doi.org/10.1021/jp003967y

Barnett, N. W. (1988). Improvements in the chemical generation of chlorine and bromine, and their respective hydrides as a means of sample introduction into an atmospheric-pressure helium microwave-induced plasma. *Journal of Analytical Atomic Spectrometry*, *3*(7), 969–972. https://doi.org/10.1039/ja9880300969

Bates, T. S., Lamb, B. K., Guenther, A., Dignon, J., & Stoiber, R. E. (1992). Sulfur emissions to the atmosphere from natural sources. *Journal of Atmospheric Chemistry*, *14*(1–4), 315–337. https://doi.org/10.1007/Bf00115242

Bertram, T. H., Kimmel, J. R., Crisp, T. A., Ryder, O. S., Yatavelli, R. L. N., Thornton, J. A., et al. (2011). A field-deployable, chemical ionization time-of-flight mass spectrometer. *Atmospheric Measurement Techniques*, *4*(7), 1471–1479. https://doi.org/10.5194/amt-4-1471-2011

Caloz, F., Seisel, S., Fenter, F. F., & Rossi, M. J. (1998). Reactivity of $BrNO_2$ and $ClNO_2$ with solid alkali salt substrates. *The Journal of Physical Chemistry. A*, *102*(38), 7470–7479. https://doi.org/10.1021/jp982000f

Chang, S. Y., & Allen, D. (2006). Atmospheric chlorine chemistry in Southeast Texas: Impacts on ozone formation and control. *Environmental Science & Technology*, *40*(1), 251–262. https://doi.org/10.1021/es050787z

Chang, S. Y., McDonald-Buller, E., Kimura, Y., Yarwood, G., Neece, J., Russell, M., et al. (2002). Sensitivity of urban ozone formation to chlorine emission estimates. *Atmospheric Environment*, *36*(32), 4991–5003. https://doi.org/10.1016/S1352-2310(02)00573-3

Crounse, J. D., McKinney, K. A., Kwan, A. J., & Wennberg, P. O. (2006). Measurement of gas-phase hydroperoxides by chemical ionization mass spectrometry. *Analytical Chemistry*, *78*(19), 6726–6732. https://doi.org/10.1021/ac0604235

D'Ambro, E. L., Lee, B. H., Liu, J., Shilling, J. E., Gaston, C. J., Lopez-Hilfiker, F. D., et al. (2017). Molecular composition and volatility of isoprene photochemical oxidation secondary organic aerosol under low- and high-NO_x conditions. *Atmospheric Chemistry and Physics*, *17*(1), 159–174. https://doi.org/10.5194/acp-17-159-2017

Day, D. A., Wooldridge, P. J., Dillon, M. B., Thornton, J. A., & Cohen, R. C. (2002). A thermal dissociation laser-induced fluorescence instrument for in situ detection of NO_2, peroxy nitrates, alkyl nitrates, and HNO_3. *Journal of Geophysical Research*, *107*(D6), 4046. https://doi.org/10.1029/2001JD000779

Faxon, C. B., Bean, J. K., & Hildebrandt Ruiz, L. (2015). Inland concentrations of Cl_2 and $ClNO_2$ in Southeast Texas suggest chlorine chemistry significantly contributes to atmospheric reactivity. *Atmosphere-Basel*, *6*(10), 1487–1506. https://doi.org/10.3390/atmos6101487

Finlayson-Pitts, B. J. (2003). The tropospheric chemistry of sea salt: A molecular-level view of the chemistry of NaCl and NaBr. *Chemical Reviews*, *103*(12), 4801–4822. https://doi.org/10.1021/cr020653t

Finlayson-Pitts, B. J. (2010). Halogens in the troposphere. *Analytical Chemistry*, *82*(3), 770–776. https://doi.org/10.1021/ac901478p

Finley, B. D., & Saltzman, E. S. (2006). Measurement of Cl_2 in coastal urban air. *Geophysical Research Letters*, *33*, L11809. https://doi.org/10.1029/2006GL025799

Foster, K. L., Caldwell, T. E., Benter, T., Langer, S., Hemminger, J. C., & Finlayson-Pitts, B. J. (1999). Techniques for quantifying gaseous HOCl using atmospheric pressure ionization mass spectrometry. *Physical Chemistry Chemical Physics*, *1*(24), 5615–5621. https://doi.org/10.1039/a907362k

Foster, K. L., Plastridge, R. A., Bottenheim, J. W., Shepson, P. B., Finlayson-Pitts, B. J., & Spicer, C. W. (2001). The role of Br_2 and BrCl in surface ozone destruction at polar sunrise. *Science*, *291*(5503), 471–474. https://doi.org/10.1126/science.291.5503.471

Friedman, B., Brophy, P., Brune, W. H., & Farmer, D. K. (2016). Anthropogenic sulfur perturbations on biogenic oxidation: SO_2 additions impact gas-phase OH oxidation products of alpha- and beta-pinene. *Environmental Science & Technology*, *50*(3), 1269–1279. https://doi.org/10.1021/acs.est.5b05010

Goldstein, A. H., & Galbally, I. E. (2007). Known and unexplored organic constituents in the Earth's atmosphere. *Environmental Science & Technology*, *41*(5), 1514–1521. https://doi.org/10.1021/es072476p

Guo, H., Sullivan, A. P., Campuzano-Jost, P., Schroder, J. C., Lopez-Hilfiker, F. D., Dibb, J. E., et al. (2016). Fine particle pH and the partitioning of nitric acid during winter in the northeastern United States. *Journal of Geophysical Research: Atmospheres*, *121*, 10,355–10,376. https://doi.org/10.1002/2016JD025311

Hegg, D. A., & Hobbs, P. V. (1981). Cloud water chemistry and the production of sulfates in clouds. *Atmospheric Environment*, *15*(9), 1597–1604. https://doi.org/10.1016/0004-6981(81)90144-X

Huey, L. G., Hanson, D. R., & Howard, C. J. (1995). Reactions of SF_6^- and I_- with atmospheric trace gases. *Journal of Physical Chemistry*, *99*(14), 5001–5008. https://doi.org/10.1021/j100014a021

Huey, L. G., Tanner, D. J., Slusher, D. L., Dibb, J. E., Arimoto, R., Chen, G., et al. (2004). CIMS measurements of HNO_3 and SO_2 at the South Pole during ISCAT 2000. *Atmospheric Environment*, *38*(32), 5411–5421. https://doi.org/10.1016/j.atmosenv.2004.04.037

Iyer, S., Lopez-Hilfiker, F., Lee, B. H., Thornton, J. A., & Kurten, T. (2016). Modeling the detection of organic and inorganic compounds using iodide-based chemical ionization. *The Journal of Physical Chemistry. A*, *120*(4), 576–587. https://doi.org/10.1021/acs.jpca.5b09837

Junninen, H., Ehn, M., Petäjä, T., Luosujärvi, L., Kotiaho, T., Kostiainen, R., et al. (2010). A high-resolution mass spectrometer to measure atmospheric ion composition. *Atmospheric Measurement Techniques*, *3*(4), 1039–1053. https://doi.org/10.5194/amt-3-1039-2010

Jurkat, T., Voigt, C., Arnold, F., Schlager, H., Aufmhoff, H., Schmale, J., et al. (2010). Airborne stratospheric ITCIMS measurements of SO_2, HCl, and HNO_3 in the aged plume of volcano Kasatochi. *Journal of Geophysical Research*, *115*, D00L17. https://doi.org/10.1029/2010JD013890

Kay, J. M., & Nedderman, R. M. (1974). *An introduction to fluid mechanics and heat transfer: with applications in chemical & mechanical process engineering*, (3d ed., Vol. xvi, p. 322). London; New York: Cambridge University Press.

Kercher, J. P., Riedel, T. P., & Thornton, J. A. (2009). Chlorine activation by N_2O_5: Simultaneous, in situ detection of $ClNO_2$ and N_2O_5 by chemical ionization mass spectrometry. *Atmospheric Measurement Techniques*, *2*(1), 193–204. https://doi.org/10.5194/amt-2-193-2009

Kim, S., Huey, L. G., Stickel, R. E., Tanner, D. J., Crawford, J. H., Olson, J. R., et al. (2007). Measurement of HO_2NO_2 in the free troposphere during the intercontinental chemical transport experiment - North America 2004. *Journal of Geophysical Research*, *112*, D12S01. https://doi.org/10.1029/2006JD007676

Kroll, J. H., Donahue, N. M., Jimenez, J. L., Kessler, S. H., Canagaratna, M. R., Wilson, K. R., et al. (2011). Carbon oxidation state as a metric for describing the chemistry of atmospheric organic aerosol. *Nature Chemistry*, *3*(2), 133–139. https://doi.org/10.1038/Nchem.948

Langner, J., & Rodhe, H. (1991). A global 3-dimensional model of the tropospheric sulfur cycle. *Journal of Atmospheric Chemistry*, *13*(3), 225–263. https://doi.org/10.1007/Bf00058134

Lawler, M. J., Sander, R., Carpenter, L. J., Lee, J. D., von Glasow, R., Sommariva, R., & Saltzman, E. S. (2011). HOCl and Cl_2 observations in marine air. *Atmospheric Chemistry and Physics*, *11*(15), 7617–7628. https://doi.org/10.5194/acp-11-7617-2011

Lee, B. H., Lopez-Hilfiker, F. D., Mohr, C., Kurten, T., Worsnop, D. R., & Thornton, J. A. (2014). An iodide-adduct high-resolution time-of-flight chemical-ionization mass spectrometer: Application to atmospheric inorganic and organic compounds. *Environmental Science & Technology*, *48*(11), 6309–6317. https://doi.org/10.1021/es500362a

Liao, J., Huey, L. G., Liu, Z., Tanner, D. J., Cantrell, C. A., Orlando, J. J., et al. (2014). High levels of molecular chlorine in the Arctic atmosphere. *Nature Geoscience*, *7*(2), 91–94. https://doi.org/10.1038/Ngeo2046

Liao, J., Sihler, H., Huey, L. G., Neuman, J. A., Tanner, D. J., Friess, U., et al. (2011). A comparison of Arctic BrO measurements by chemical ionization mass spectrometry and long path-differential optical absorption spectroscopy. *Journal of Geophysical Research*, *116*, D00R02. https://doi.org/10.1029/2010JD014788

Lopez-Hilfiker, F. D., Constantin, K., Kercher, J. P., & Thornton, J. A. (2012). Temperature dependent halogen activation by N_2O_5 reactions on halide-doped ice surfaces. *Atmospheric Chemistry and Physics*, *12*(11), 5237–5247. https://doi.org/10.5194/acp-12-5237-2012

Lopez-Hilfiker, F. D., Iyer, S., Mohr, C., Lee, B. H., L, E., D'Ambro, T. K., & Thornton, J. A. (2016). Constraining the sensitivity of iodide adduct chemical ionization mass spectrometry to multifunctional organic molecules using the collision limit and thermodynamic stability of iodide ion adducts. *Atmospheric Measurement Techniques*, *9*(4), 1505–1512. https://doi.org/10.5194/amt-9-1505-2016

Lopez-Hilfiker, F. D., Mohr, C., D'Ambro, E. L., Lutz, A., Riedel, T. P., Gaston, C. J., et al. (2016). Molecular composition and volatility of organic aerosol in the southeastern US: Implications for IEPDX derived SOA. *Environmental Science & Technology*, *50*(5), 2200–2209. https://doi.org/10.1021/acs.est.5b04769

Luke, W. T. (1997). Evaluation of a commercial pulsed fluorescence detector for the measurement of low-level SO_2 concentrations during the gas-phase sulfur intercomparison experiment. *Journal of Geophysical Research*, *102*, 16,255–16,265. https://doi.org/10.1029/96JD03347

Marcy, T. P., Gao, R. S., Northway, M. J., Popp, P. J., Stark, H., & Fahey, D. W. (2005). Using chemical ionization mass spectrometry for detection of HNO_3, HOI, and $ClONO_2$ in the atmosphere. *International Journal of Mass Spectrometry*, *243*(1), 63–70. https://doi.org/10.1016/j.ijms.2004.11.012

Matsumi, Y., Shigemori, H., & Takahashi, K. (2005). Laser-induced fluorescence instrument for measuring atmospheric SO_2. *Atmospheric Environment*, *39*(17), 3177–3185. https://doi.org/10.1016/j.atmosenv.2005.02.023

McCulloch, A., Aucott, M. L., Benkovitz, C. M., Graedel, T. E., Kleiman, G., Midgley, P. M., & Li, Y. F. (1999). Global emissions of hydrogen chloride and chloromethane from coal combustion, incineration and industrial activities: Reactive Chlorine Emissions Inventory. *Journal of Geophysical Research*, *104*, 8391–8403. https://doi.org/10.1029/1999JD900025

McNeill, V. F., Patterson, J., Wolfe, G. M., & Thornton, J. A. (2006). The effect of varying levels of surfactant on the reactive uptake of N_2O_5 to aqueous aerosol. *Atmospheric Chemistry and Physics*, *6*(6), 1635–1644. https://doi.org/10.5194/acp-6-1635-2006

Miake-Lye, R. C., Anderson, B. E., Cofer, W. R., Wallio, H. A., Nowicki, G. D., Ballenthin, J. O., et al. (1998). SO_x oxidation and volatile aerosol in aircraft exhaust plumes depend on fuel sulfur content. *Geophysical Research Letters*, *25*, 1677–1680. https://doi.org/10.1029/98GL00064

Mielke, L. H., Furgeson, A., & Osthoff, H. D. (2011). Observation of $ClNO_2$ in a mid-continental urban environment. *Environmental Science & Technology*, *45*(20), 8889–8896. https://doi.org/10.1021/es201955u

Mohler, O., Reiner, T., & Arnold, F. (1992). The formation of SO_5^- by gas-phase ion-molecule reactions. *The Journal of Chemical Physics*, *97*(11), 8233–8239. https://doi.org/10.1063/1.463394

Mohr, C., Lopez-Hilfiker, F. D., Yli-Juuti, T., Heitto, A., Lutz, A., Hallquist, M., et al. (2017). Ambient observations of dimers from terpene oxidation in the gas phase: Implications for new particle formation and growth. *Geophysical Research Letters*, *44*, 2958–2966. https://doi.org/10.1002/2017GL072718

Neuman, J. A., Nowak, J. B., Huey, L. G., Burkholder, J. B., Dibb, J. E., Holloway, J. S., et al. (2010). Bromine measurements in ozone depleted air over the Arctic Ocean. *Atmospheric Chemistry and Physics*, *10*(14), 6503–6514. https://doi.org/10.5194/acp-10-6503-2010

Okabe, H., Splitstone, P. L., & Ball, J. J. (1973). Ambient and source SO_2 detector based on a fluorescence method. *Journal of the Air Pollution Control Association*, *23*(6), 514–516.

Orlando, J. J., & Burkholder, J. B. (1995). Gas-phase UV visible absorption-spectra of HOBr and Br_2O. *The Journal of Physical Chemistry*, *99*(4), 1143–1150. https://doi.org/10.1021/j100004a013

Osthoff, H. D., Roberts, J. M., Ravishankara, A. R., Williams, E. J., Lerner, B. M., Sommariva, R., et al. (2008). High levels of nitryl chloride in the polluted subtropical marine boundary layer. *Nature Geoscience*, *1*(5), 324–328. https://doi.org/10.1038/ngeo177

Platt, U., & Hönninger, G. (2003). The role halogens species in the troposphere. *Chemosphere*, *52*(2), 325–338. https://doi.org/10.1016/S0045-6535(03)00216-9

Ridley, B., Ott, L., Pickering, K., Emmons, L., Montzka, D., Weinheimer, A., et al. (2004). Florida thunderstorms: A faucet of reactive nitrogen to the upper troposphere. *Journal of Geophysical Research*, *109*, D17305. https://doi.org/10.1029/2004JD004769

Riedel, T. P., Bertram, T. H., Crisp, T. A., Williams, E. J., Lerner, B. M., Vlasenko, A., et al. (2012). Nitryl chloride and molecular chlorine in the coastal marine boundary layer. *Environmental Science & Technology*, *46*(19), 10,463–10,470. https://doi.org/10.1021/es204632r

Riedel, T. P., Wagner, N. L., Dubé, W. P., Middlebrook, A. M., Young, C. J., Öztürk, F., et al. (2013). Chlorine activation within urban or power plant plumes: Vertically resolved $ClNO_2$ and Cl_2 measurements from a tall tower in a polluted continental setting. *Journal of Geophysical Research: Atmospheres*, *118*, 8702–8715. https://doi.org/10.1002/jgrd.50637

Riedel, T. P., Wolfe, G. M., Danas, K. T., Gilman, J. B., Kuster, W. C., Bon, D. M., et al. (2014). An MCM modeling study of nitryl chloride ($ClNO_2$) impacts on oxidation, ozone production and nitrogen oxide partitioning in polluted continental outflow. *Atmospheric Chemistry and Physics*, *14*(8), 3789–3800. https://doi.org/10.5194/acp-14-3789-2014

Roberts, J. M., Osthoff, H. D., Brown, S. S., & Ravishankara, A. R. (2008). N_2O_5 oxidizes chloride to Cl_2 in acidic atmospheric aerosol. *Science*, *321*(5892), 1059–1059. https://doi.org/10.1126/science.1158777

Roberts, J. M., Veres, P., Warneke, C., Neuman, J. A., Washenfelder, R. A., Brown, S. S., et al. (2010). Measurement of HONO, HNCO, and other inorganic acids by negative-ion proton-transfer chemical-ionization mass spectrometry (NI-PT-CIMS): Application to biomass burning emissions. *Atmospheric Measurement Techniques*, *3*(4), 981–990. https://doi.org/10.5194/amt-3-981-2010

Rollins, A. W., Thornberry, T. D., Ciciora, S. J., McLaughlin, R. J., Watts, L. A., Hanisco, T. F., et al. (2016). A laser-induced fluorescence instrument for aircraft measurements of sulfur dioxide in the upper troposphere and lower stratosphere. *Atmospheric Measurement Techniques*, *9*(9), 4601–4613. https://doi.org/10.5194/amt-9-4601-2016

Rossi, M. J. (2003). Heterogeneous reactions on salts. *Chemical Reviews*, *103*(12), 4823–4882. https://doi.org/10.1021/cr020507n

Ryerson, T. B., Buhr, M. P., Frost, G. J., Goldan, P. D., Holloway, J. S., Hübler, G., et al. (1998). Emissions lifetimes and ozone formation in power plant plumes. *Journal of Geophysical Research*, *103*, 22,569–22,583. https://doi.org/10.1029/98JD01620

Saiz-Lopez, A., & von Glasow, R. (2012). Reactive halogen chemistry in the troposphere. *Chemical Society Reviews*, *41*(19), 6448–6472. https://doi.org/10.1039/c2cs35208g

Sarwar, G., Simon, H., Xing, J., & Mathur, R. (2014). Importance of tropospheric $ClNO_2$ chemistry across the Northern Hemisphere. *Geophysical Research Letters*, *41*, 4050–4058. https://doi.org/10.1002/2014GL059962

Schobesberger, S., Lopez-Hilfiker, F. D., Taipale, D., Millet, D. B., D'Ambro, E. L., Rantala, P., et al. (2016). High upward fluxes of formic acid from a boreal forest canopy. *Geophysical Research Letters*, *43*, 9342–9351. https://doi.org/10.1002/2016GL069599

Schwarz, F. P., Okabe, H., & Whittaker, J. K. (1974). Fluorescence detection of sulfur dioxide in air at parts per billion level. *Analytical Chemistry*, *46*(8), 1024–1028. https://doi.org/10.1021/ac60344a002

Seeley, J. V., Morris, R. A., & Viggiano, A. A. (1997). Rate constants for the reactions of CO_3-(H_2O)(n=0-5)+SO_2: Implications for CIMS detection of SO_2. *Geophysical Research Letters*, *24*, 1379–1382. https://doi.org/10.1029/97GL01323

Simeonsson, J. B., Matta, A., & Boddeti, R. (2012). Direct measurement of SO_2 in air by laser induced fluorescence spectrometry using a nontunable laser source. *Analytical Letters*, *45*(8), 894–906. https://doi.org/10.1080/00032719.2012.655681

Simpson, W. R., Brown, S. S., Saiz-Lopez, A., Thornton, J. A., & von Glasow, R. (2015). Tropospheric halogen chemistry: Sources, cycling, and impacts. *Chemical Reviews*, *115*(10), 4035–4062. https://doi.org/10.1021/cr5006638

Sipila, M., Berndt, T., Petaja, T., Brus, D., Vanhanen, J., Stratmann, F., et al. (2010). The role of sulfuric acid in atmospheric nucleation. *Science*, *327*(5970), 1243–1246. https://doi.org/10.1126/science.1180315

Slusher, D. L., Huey, L. G., Tanner, D. J., Flocke, F. M., & Roberts, J. M. (2004). A thermal dissociation-chemical ionization mass spectrometry (TD-CIMS) technique for the simultaneous measurement of peroxyacyl nitrates and dinitrogen pentoxide. *Journal of Geophysical Research*, *109*, D19315. https://doi.org/10.1029/2004JD004670

Smith, S. J., van Aardenne, J., Klimont, Z., Andres, R. J., Volke, A., & Arias, S. D. (2011). Anthropogenic sulfur dioxide emissions: 1850-2005. *Atmospheric Chemistry and Physics*, *11*(3), 1101–1116. https://doi.org/10.5194/acp-11-1101-2011

Speidel, M., Nau, R., Arnold, F., Schlager, H., & Stohl, A. (2007). Sulfur dioxide measurements in the lower, middle and upper troposphere: Deployment of an aircraft-based chemical ionization mass spectrometer with permanent in-flight calibration. *Atmospheric Environment*, *41*(11), 2427–2437. https://doi.org/10.1016/j.atmosenv.2006.07.047

Spicer, C. W., Chapman, E. G., Finlayson-Pitts, B. J., Plastridge, R. A., Hubbe, J. M., Fast, J. D., & Berkowitz, C. M. (1998). Unexpectedly high concentrations of molecular chlorine in coastal air. *Nature*, *394*(6691), 353–356. https://doi.org/10.1038/28584

Tanaka, P. L., Riemer, D. D., Chang, S., Yarwood, G., McDonald-Buller, E. C., Apel, E. C., et al. (2003). Direct evidence for chlorine-enhanced urban ozone formation in Houston, Texas. *Atmospheric Environment*, *37*(9–10), 1393–1400. https://doi.org/10.1016/S1352-2310(02)01007-5

Thornton, D. C., Bandy, A. R., Tu, F. H., Blomquist, B. W., Mitchell, G. M., Nadler, W., & Lenschow, D. H. (2002). Fast airborne sulfur dioxide measurements by Atmospheric Pressure Ionization Mass Spectrometry (APIMS). *Journal of Geophysical Research*, *107*(D22), 4632. https://doi.org/10.1029/2002jd002289

Thornton, J. A., & Abbatt, J. P. D. (2005). N_2O_5 reaction on submicron sea salt aerosol: Kinetics, products, and the effect of surface active organics. *The Journal of Physical Chemistry. A*, *109*(44), 10,004–10,012. https://doi.org/10.1021/jp054183t

Thornton, J. A., Kercher, J. P., Riedel, T. P., Wagner, N. L., Cozic, J., Holloway, J. S., et al. (2010). A large atomic chlorine source inferred from mid-continental reactive nitrogen chemistry. *Nature*, *464*(7286), 271–274. https://doi.org/10.1038/nature08905

Wagner, N. L., Dube, W. P., Washenfelder, R. A., Young, C. J., Pollack, I. B., Ryerson, T. B., & Brown, S. S. (2011). Diode laser-based cavity ring-down instrument for NO_3, N_2O_5, NO, NO_2 and O_3 from aircraft. *Atmospheric Measurement Techniques*, *4*(6), 1227–1240. https://doi.org/10.5194/amt-4-1227-2011

Wang, T., Tham, Y. J., Xue, L., Li, Q., Zha, Q., Wang, Z., et al. (2016). Observations of nitryl chloride and modeling its source and effect on ozone in the planetary boundary layer of southern China. *Journal of Geophysical Research: Atmospheres*, *121*, 2476–2489. https://doi.org/10.1002/2015JD024556

Weber, R. J., Guo, H. Y., Russell, A. G., & Nenes, A. (2016). High aerosol acidity despite declining atmospheric sulfate concentrations over the past 15 years. *Nature Geoscience*, *9*(4), 282–285. https://doi.org/10.1038/Ngeo2665

Wild, R. J., Edwards, P. M., Dubé, W. P., Baumann, K., Edgerton, E. S., Quinn, P. K., et al. (2014). A measurement of total reactive nitrogen, NO_y, together with NO_2, NO, and O_3 via cavity ring-down spectroscopy. *Environmental Science & Technology*, *48*(16), 9609–9615. https://doi.org/10.1021/es501896w

Wojcik, G. S., & Chang, J. S. (1997). A re-evaluation of sulfur budgets, lifetimes, and scavenging ratios for eastern North America. *Journal of Atmospheric Chemistry*, *26*(2), 109–145. https://doi.org/10.1023/A:1005848828770

Wooldridge, P. J., Perring, A. E., Bertram, T. H., Flocke, F. M., Roberts, J. M., Singh, H. B., et al. (2010). Total peroxy nitrates (sigma PNs) in the atmosphere: The thermal dissociation-laser induced fluorescence (TD-LIF) technique and comparisons to speciated PAN measurements. *Atmospheric Measurement Techniques*, *3*(3), 593–607. https://doi.org/10.5194/amt-3-593-2010

Yatavelli, R. L. N., Lopez-Hilfiker, F., Wargo, J. D., Kimmel, J. R., Cubison, M. J., Bertram, T. H., et al. (2012). A chemical ionization high-resolution time-of-flight mass spectrometer coupled to a micro orifice volatilization impactor (MOVI-HRToF-CIMS) for analysis of gas and particle-phase organic species. *Aerosol Science and Technology*, *46*(12), 1313–1327. https://doi.org/10.1080/02786826.2012.712236

Young, C. J., Washenfelder, R. A., Roberts, J. M., Mielke, L. H., Osthoff, H. D., Tsai, C., et al. (2012). Vertically resolved measurements of nighttime radical reservoirs; in Los Angeles and their contribution to the urban radical budget. *Environmental Science & Technology*, *46*(20), 10,965–10,973. https://doi.org/10.1021/es302206a